Chin. Geogra. Sci. 2022 Vol. 32 No. 4 pp. 676−685
https://doi.org/10.1007/s11769-022-1293-1

Springer Science Press
www.springerlink.com/content/1002-0063

Soil Salinity and Soil Water Content Estimation Using Digital Images in Coastal Field: A Case Study in Yancheng City of Jiangsu Province, China

XU Lu[1], MA Hongyuan[2], WANG Zhichun[2]

(1. *School of Geography, Geomatics and Planning, Jiangsu Normal University, Xuzhou* 221116, *China*; 2. *Northeast Institute of Geography and Agroecology, Chinese Academy of Sciences, Changchun* 130012, *China*)

Abstract: Soil is the essential part for agricultural and environmental sciences, and soil salinity and soil water content are both the important influence factors for sustainable development of agriculture and ecological environment. Digital camera, as one of the most popular and convenient proximal sensing instruments, has its irreplaceable position for soil properties assessment. In this study, we collected 52 soil samples and photographs at the same time along the coast in Yancheng City of Jiangsu Province. We carefully analyzed the relationship between soil properties and image brightness, and found that soil salt content had higher correlation with average image brightness value than soil water content. From the brightness levels, the high correlation coefficients between soil salt content and brightness levels concentrated on the high brightness values, and the high correlation coefficients between soil water content and brightness levels focused on the low brightness values. Different significance levels (*P*) determined different brightness levels related to soil properties, hence *P* value setting can be an optional way to select brightness levels as the input variables for modeling soil properties. Given these information, random forest algorithm was applied to develop soil salt content and soil water content inversion models using randomly 70% of the dataset, and the rest data for testing models. The results showed that soil salt content model had high accuracy (R_v^2 = 0.79, $RMSE_v$ = 12 g/kg, and RPD_v = 2.18), and soil water content inversion model was barely satisfied (R_v^2 = 0.47, $RMSE_v$ = 3.04%, and RPD_v = 1.38). This study proposes a method of modeling soil properties with a digital camera. Combining unmanned aerial vehicle (UAV), it has potential popularization and application value for precise agriculture and land management.

Keywords: soil salinity; soil water content; coastal soil; digital image

Citation: XU Lu, MA Hongyuan, WANG Zhichun, 2022. Soil Salinity and Soil Water Content Estimation Using Digital Images in Coastal Field: A Case Study in Yancheng City of Jiangsu Province, China. *Chinese Geographical Science*, 32(4): 676−685. https://doi.org/10.1007/s11769-022-1293-1

1 Introduction

Soil salinization is one of the global problems for soil degradation. It not only affects agricultural sustainable development, but also causes certain damage to the ecological environment (Qadir et al., 2001). Due to the change of natural environment and the influence of human activities, the degree and distribution of soil salinization have been changing all the time. Therefore, accurate monitoring of soil salinization is an important prerequisite for scientific management and rational utilization of saline soil (Metternicht and Zinck, 2003). The

Received date: 2021-10-27; accepted date: 2022-02-25

Foundation item: Under the auspices of the Strategic Priority Research Program of the Chinese Academy of Sciences (No. XDA28110301, XDA2306040303), National Natural Science Foundation of China (No. 41807001, 41977424), Natural Science Foundation of Jilin Province (No. 20200201026JC)

Corresponding author: MA Hongyuan. E-mail: mahongyuan@iga.ac.cn

traditional method of soil salinization monitoring needs a lot of manpower, material resources and time cost, and the sampling time and area have certain limits. It is difficult to realize the rapid update of soil salinization monitoring (Metternicht and Zinck, 2008). Remote sensing quantitative estimation has been widely considered as a convenient and fast new method (Ivushkin et al., 2019; Yang and Guo, 2019; Wang et al., 2020). However, remote sensing still has some limitations, such as unsuitable for small-scale area, susceptible to weather condition, hard to use whenever and wherever possible and so on.

Soil water content is an important parameter for influencing the exchange of energy and mass between atmosphere and land surface, irrigation management and ecosystem function (Barrett et al., 2009; Wang and Qu, 2009; Wulf et al., 2014). Traditional approaches for soil water measurement are generally time consuming, laborious, destructive and only provide point data. Remote sensing technology provides a convenient way to estimate soil water content and map its spatial distribution for continuous temporal coverage at regional and global scales (Wang and Qu, 2009; Yashchenko and Bobrov, 2016). Although, soil water content is widely studied with remote sensing data from optical to microwave domains at various spatial scales (Su et al., 2016; Yue et al., 2019), remote sensing data still have some drawbacks as mentioned above. Therefore, proximal soil sensing is a convenient and effective measurement to monitor soil properties for fine scale and real-time monitoring (Adamchuk et al., 2015; Viscarra Rossel et al., 2010).

Proximal soil sensing, a nondestructive and field-scale technique, could fill the gap between traditional measurement and remote sensing methods (Adamchuk and Rossel, 2011). Many instruments, including ground-penetrating radar (GPR), electromagnetic induction (EMI), portable *X*-ray fluorescence (P-XRF), time domain reflectometry (TDR), optical reflectance (UV/Vis/NIR/MIR), and gamma-ray spectroscopy, are effective and convenient for estimating soil properties in complex field conditions, but they are mostly used in scientific researches for their expensive cost and complex operation (Adamchuk et al., 2015; Viscarra Rossel and Bouma, 2016). Comparatively, digital camera is easily accepted as a soil monitoring tool for its popularity in our daily life. Digital cameras have successfully been attempted to study soil parameters, such as soil organic carbon (Wu et al., 2018; Fu et al., 2019), soil iron content (Viscarra Rossel et al., 2008), soil structure (Puzachenko et al., 2004), soil water content (Persson, 2005; Zanetti et al., 2015), and soil salinity (Ren et al., 2016; Xu et al., 2020). However, most studies were conducted in the laboratory or under limited field conditions, which largely impeded the practical application for complex field conditions. In addition, Farifteh (2011) pointed out that soil water content and soil salinity interfering each other on soil spectra made it difficult to accurately estimate themselves with soil spectra. Digital images are made up of three colors, which can be derived from soil spectra (Islam et al., 2004). Hence soil water content and soil salinity could also impact each other on the digital images, and lead to the difficulty in determining soil properties with soil images. Nowadays it is still a challenging scientific research problem to overcome.

Digital images reflect comprehensive information of soil surface, and we assume that image brightness is mainly affected by the most important influence factors, soil salinity and soil water content. In the present study, we conduct the experiment in actual field conditions, including soil sampling and soil photography, and take advantages of random forest algorithm to explore the relationship within soil properties and digital images. The objective is to build models for precisely estimating soil salinity and soil water content in complex field condition using soil digital images. This study has potential application value for precision agriculture and the method can be applied to predict other soil properties.

2 Materials and Methods

2.1 Study area

The study area is located in the coast area of Yancheng City of Jiangsu Province (120.52°N–120.86°N, 33.03°E–33.5°E). This area experiences the subtropical ocean monsoon climate, influenced by continental and marine climates. The annual precipitation is about 900–1000 mm, and the annual temperature is about 13.7°C–14.8°C (Fang et al., 2015). Seawater infiltration leads to groundwater with higher mineralization, and improper utilization of human activities makes shallow saline groundwater rise to the surface, resulting in the increasing soil salinization. Salinization degrades soil quality and makes it difficult to use, so the coastal land is

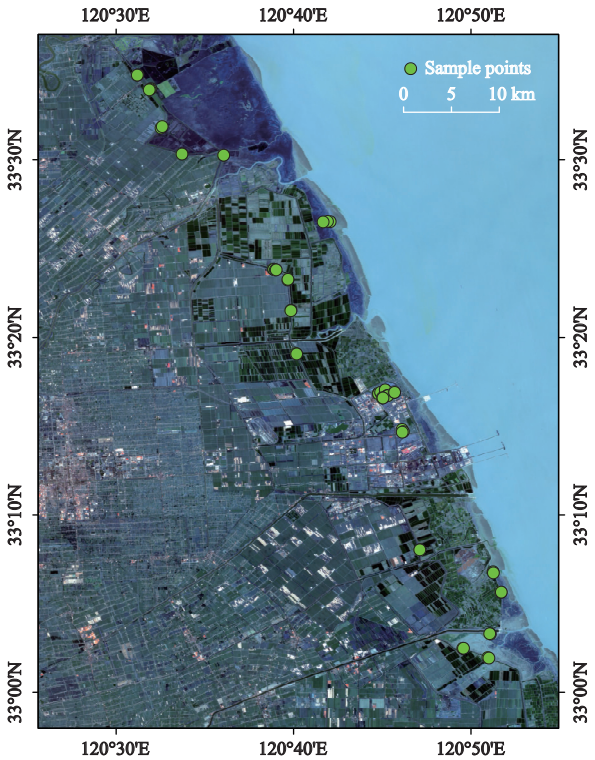

Fig. 1 Location of study area and sampling points in Yancheng City of Jiangsu Province, China

mainly aquaculture land and reclamation area (Werner et al., 2013). Fig. 1 showed the study area and sampling sites.

2.2 Field survey

We conducted a field survey for three days on August 2018, and the weather at that time were mostly sunny and a little windy. We drove along the coastline and chose the bare soil surface with different states for photographing and sampling. To increase the complexity of digital image data for developing robust models, we photographed and sampled a total of 52 sites all day long at the sunny and cloudy weather conditions (Fig. 2).

In this field survey, Cannon EOS 760D digital camera with a resolution of 6000 × 4000 pixels was used to take photos. The shooting process is as follows. Firstly, we chose a piece of bare land without the interference of vegetation and other sundry objects. Secondly, height of the camera from the ground was adjusted to keep the bare land area covering the whole field of view (FOV) of the camera. Finally, digital images were captured at automatic mode with the lens perpendicular to the ground. Automatic mode would prevent incorrect camera focusing and exposure time, and help to obtain

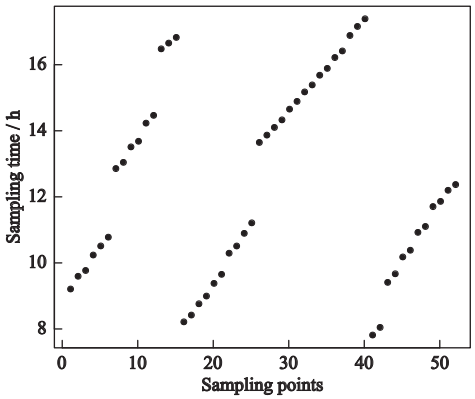

Fig. 2 Sampling time for each sampling point in the coast area of Yancheng City of Jiangsu Province, China in 2018

stable photo quality under various ambient light background in the field (Aitkenhead et al., 2016). Digital images were saved in JPG format. After obtaining soil images, we collected the top soil (about 0–5 cm) and immediately put the soil into a plastic bag. The sampled soils were kept sealed and stored in a dry box until we measured their wet weight in the same day. At the same time the location of sampling points was recorded.

2.3 Laboratory analysis

After carrying the soil samples into the laboratory, we put them in the oven at 105°C for 24 h to obtain the dry weight. Soil water content is obtained via soil dry weight and wet weight (Jackson, 2005). Soil salt content (SSC) was measured via dry evaporation methods (Rhoades and Ingvalson, 1971). To solve the edge deformation problem of digital images, we cut off the 20% of the image edges, and only consider the central part of the soil images. Digital images in JPG format could be divided into three color components (RGB) and also could be converted to grayscale (Gr). The value range of four color components (R, G, B, Gr) is 0–255. Table 1 gives the summary statistics of soil color components and soil properties.

2.4 Correlation analysis

After we got the soil properties and soil color component information. We calculated the mean of soil image brightness for each sample, and analyzed the correlation coefficient between soil properties and average brightness. Besides, we further analyzed the relationship between soil properties and each brightness level of four color components. The correlation coefficient can be calculated as follow (Wang et al., 2019).

Table 1 Summary of soil color components and soil properties (n = 52)

Soil property	Min.	Median	Mean	Max.	SD	CV
R	59.72	224.12	206.6	250.12	45.18	0.22
G	54.99	210.68	193.74	244.07	44.56	0.23
B	49.03	193.56	178.94	234.35	44.5	0.25
Gr	54.98	210.02	193.09	242.85	44.55	0.23
SSC	0.80	78.87	68.21	131.26	34.62	0.51
SWC	4.06	18.33	18.57	43.88	7.69	0.41

Notes: SD, standard deviation; CV, coefficient of variation; SWC / %, unit of soil water content; SSC / (g/kg), unit of soil salt content, R, G, B and Gr mean red, green, blue, and gray. Hereinafter inclusive

$$r = \frac{\sum (x-\bar{x})(y-\bar{y})}{\sqrt{\sum (x-\bar{x})^2 \sum (y-\bar{y})^2}} \tag{1}$$

where, r means correlation coefficient, x and y are two variables, $\bar{x}$ and $\bar{y}$ are the average value of x and y.

2.5 Modeling and validation

Each image has at most 256 brightness levels, and each brightness level has a lot of pixels. We counted the pixel number at each brightness level and calculated their proportion to all pixels in an image. For each soil sample, we get soil properties and the pixel proportion of 256 brightness values. However, not all the brightness levels are helpful to model soil properties, so we need to distinguish useful ones from all the brightness levels.

We analyzed the relationship between soil properties and pixel proportion of all brightness values, and found the significantly correlated brightness values. The significance level (P) can be set at $P < 0.05$, $P < 0.01$ and $P < 0.001$. For different significance levels, there will be different correlated brightness levels chosen as the input variables. To test the accuracy of models, we split randomly 70% of dataset as the training data, the rest as the testing data. After standardizing the training data, we applied the random forest algorithm to build the prediction models.

Random forest algorithm is an ensemble learning method that generates many trees (Breiman, 2001). All the trees are trained with the training data by the method of bootstrap sampling, and the accuracy is verified by out-of- bag samples. The algorithm has two main parameters, namely number of decision trees (*ntree*) and node number (*mtry*). In this study, the two parameters are set to the default values. We applied 10-fold cross-validation method to verify the accuracy and repeated 10 times to calculated the average value as the final prediction. Then we tested the validation of models with the testing data, and repeated 100 times to identify the optimal models.

In addition, the determining coefficient (R^2), root mean square error (*RMSE*) and the ratio of performance to deviation (*RPD*) are employed to evaluate the performance of models with both training data and testing data (Xu et al., 2020).

$$R^2 = 1 - \frac{\sum_{i=1}^{n} (P_i - O_i)^2}{\sum_{i=1}^{n} (P_i - \overline{O})^2} \tag{2}$$

$$RMSE = \sqrt{\frac{1}{n} \sum_{i=1}^{n} (P_i - O_i)^2} \tag{3}$$

$$RPD = \sqrt{\frac{\sum_{i=1}^{n} (O_i - \overline{O})^2}{n \times RMSE}} \tag{4}$$

where O means the observed data, P means the predicted data, $\overline{O}$ means the mean of observed data, i means the order of each data, n means the number of all data.

Generally, models with a higher R^2 and a lower *RMSE* have better predictive power. Models with *RPD* > 2 have good predictability. Models with 2 > *RPD* > 1.4 have comparatively general predictability, and models with *RPD* < 1.4 have less reliable predictability (Chang et al., 2001).

3 Results

3.1 The relationship between soil properties and soil brightness

Soil salt content was significantly relative with the aver-

age image brightness values, and soil water content was insignificantly relative with them (Fig. 3). Also the relationship between soil salt content and soil water content was relatively weak (r = 0.29) but reached a significant level (P < 0.05). The relationship among the average brightness values of four color components was highly relative with each other.

3.2 The relationship between soil properties and each brightness level

For soil salt content, it has highly significant correlation with four color components for many brightness levels, and the best correlation coefficient reached negatively 0.56 at 150 brightness value (P < 0.001) and positively 0.53 at 221 brightness value (P < 0.001). Particularly worth mentioning is that there are generally two brightness ranges closely related with soil salt content, negative correlation at about 110–160 and positive correlation at about 220–250 brightness range (Fig. 4a).

Different from the average brightness value, soil water content has significantly relationship with some brightness levels for each color component. For the best positive correlations, soil water content was highly re-

	R	G	B	Gr	SSC	SWC
R	1.00	0.99	0.97	0.99	0.42	0.06
G	0.99	1.00	0.99	1.00	0.46	0.04
B	0.97	0.99	1.00	0.99	0.51	0.04
Gr	0.99	1.00	0.99	1.00	0.47	0.05
SSC	0.42	0.46	0.51	0.47	1.00	0.29
SWC	0.06	0.04	0.04	0.05	0.29	1.00

Fig. 3 Correlation coefficient between soil properties and average brightness values in the coast area of Yancheng City of Jiangsu Province, China. R, G, B and Gr mean red, green, blue and gray. SSC and SWC represent soil salt content and soil water content

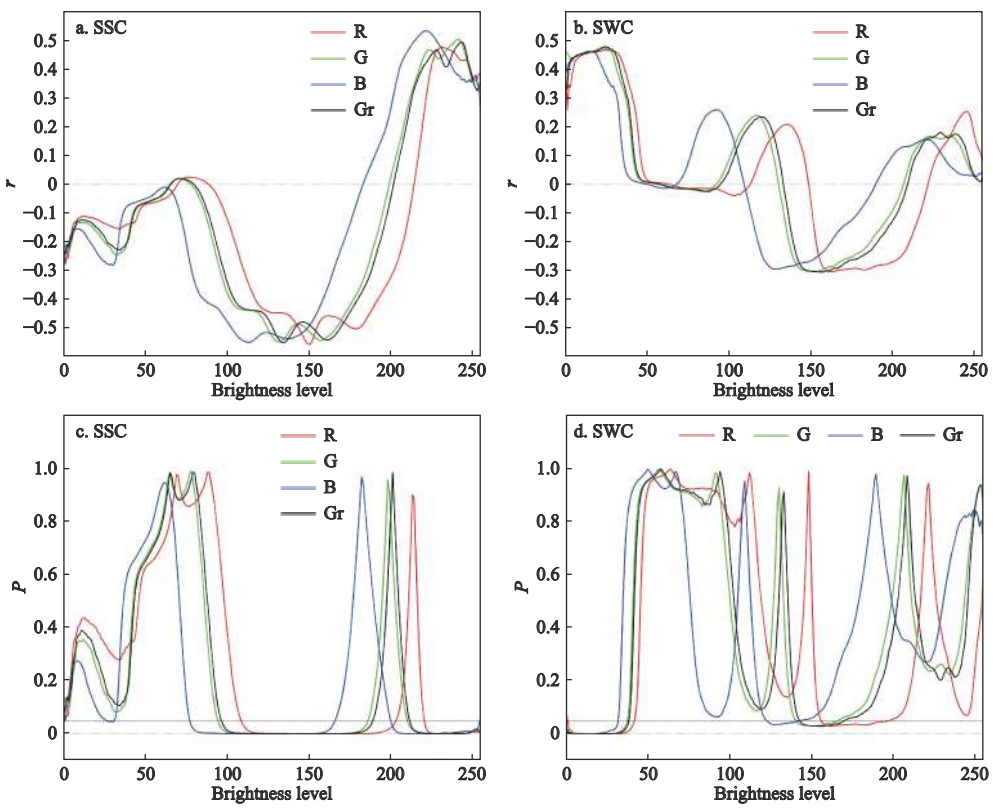

Fig. 4 Correlation coefficient (r) between brightness levels and (a) soil salt content and (b) soil water content for each color component in the coast area of Yancheng City of Jiangsu Province, China. the dotted line is r = 0; significance analysis (P) between brightness levels and (c) soil salt content and (d) soil water content for each color component, the dotted line is P = 0.05. R, G, B and Gr mean red, green, blue and gray. SSC and SWC represent soil salt content and soil water content

lated to R, G, B and Gr color components at the brightness value 24 (r = 0.468, P < 0.001), 22 (r = 0.476, P < 0.001), 15 (r = 0.463, P < 0.001), and 24 (r = 0.479, P < 0.001) respectively. As for the best negative correlations, soil water content was closely correlative with R, G, B and Gr color components at the brightness value 161 (r = –0.303, P = 0.029), 150 (r = –0.302, P = 0.03), 127 (r = –0.293, P = 0.035), and 157 (r = –0.304, P = 0.028) respectively. By contrast, the best correlations were mainly concentrated at the 10–30 brightness range (Fig. 4b).

Many brightness levels at about 80–250 were significantly relative with soil salt content, while only a few brightness levels at about 0–40 were significantly relative with soil water content (Figs. 4c and 4d).

3.3 Modeling process

Based on the above results, we knew that there were many useless brightness levels less relevant to soil properties. Brightness levels selection was hence a necessary step to confirm the relevant variables for modeling. As mentioned earlier, significance analysis provided the correlative brightness levels for four color components, so we determined the relevant variables with P value. In this study, we tried three P values (0.05, 0.01, and 0.001), and calculated the number of brightness levels for four color components at each P value (Table 2). For each P value and color component, one set of data, including soil properties and image brightness data, were generated for modeling and validation. Due to three P values and four color components, there would be twelve (3 × 4 = 12) datasets for modeling each soil property.

All four color components had enough ability to develop predictable models for soil salt content estimation, and the best one was confirmed with blue color component and at P = 0.05 level. While for soil water content estimation, all four color components could build moderately predictable models with training data, but they were difficult to satisfy the testing data. Under compares, we chose the optimal model with gray color component and at P = 0.01 level for evaluating soil water content (Table 3).

Soil salt content inversion model had a higher accuracy with a R^2 of 0.79, a *RMSE* of 12 g/kg, and a *RPD* of 2.18 for testing data, and the soil water content prediction model had a comparatively lower accuracy with a R^2 of 0.47, a *RMSE* of 3.04 %, and a *RPD* of 1.38 for testing data (Fig. 5).

4 Discussion

4.1 Effects of soil properties on soil photographs

As far as we know, soil salt rises to the land surface with soil water evaporation, and enhances the surface soil reflection, which can be reflected in the increased brightness of the photograph (Xu et al., 2019; Xu et al., 2020). Soil water content will lower the soil surface brightness and should be negatively related to the image brightness value (Persson, 2005; Zhu et al., 2011). In this study, soil salt content has significantly positive correlation with the average brightness values, and soil water content has the insignificantly positive correlation with them. Different from previous studies, the main composition of the costal soil salt is sodium chloride (NaCl), and the salt type will form a thin and smooth crystal film on the soil surface during the natural evaporation process (Xu et al., 2020). This crystal structure,

Table 2 Related brightness levels for four color components at three significant levels

Soil property	P	Brightness levels			
		R	G	B	Gr
SSC	*	131	137	151	136
	**	116	119	129	118
	***	75	76	85	69
SWC	*	83	64	54	66
	**	36	34	27	34
	***	25	27	14	26

Notes: R, G, B and Gr mean red, green, blue and gray. SSC and SWC represent soil salt content and soil water content. * means P < 0.05, ** means P < 0.01, *** means P < 0.001

Table 3 Summary of models with each color component at each *P* value

Soil property	Color component	*P*	R^2_m	$RMSE_m$ / (g/kg)	RPD_m	R^2_v	$RMSE_v$ / (g/kg)	RPD_v
SSC	R	*	0.83	12.20	2.42	0.69	14.77	1.81
		**	0.79	12.45	2.18	0.60	17.26	1.58
		***	0.67	14.02	1.75	0.25	20.99	1.16
	G	*	0.65	14.09	1.69	0.66	15.18	1.71
		**	0.69	13.95	1.81	0.54	17.22	1.47
		***	0.60	14.34	1.59	0.48	17.85	1.38
	B	*	**0.88**	**10.64**	**2.84**	**0.79**	**12.00**	**2.18**
		**	0.76	13.86	2.05	0.68	12.55	1.76
		***	0.72	14.44	1.91	0.45	18.65	1.35
	Gr	*	0.74	14.10	1.97	0.68	15.32	1.77
		**	0.68	14.74	1.78	0.58	15.46	1.53
		***	0.67	15.15	1.75	0.58	16.48	1.54
SWC	R	*	0.56	3.68	1.51	0.26	4.43	1.16
		**	0.60	3.44	1.59	0.10	4.15	1.05
		***	0.57	3.54	1.52	–0.07	3.79	0.96
	G	*	0.38	3.53	1.27	–0.68	8.90	0.77
		**	0.62	3.64	1.62	–0.05	4.11	0.98
		***	0.57	3.76	1.53	0.30	2.44	1.20
	B	*	0.09	4.41	1.05	0.05	3.81	1.03
		**	0.26	4.40	1.17	0.13	2.93	1.07
		***	–0.05	4.58	0.98	–0.35	3.94	0.86
	Gr	*	0.57	3.70	1.52	–0.16	4.02	0.93
		**	**0.61**	**3.60**	**1.60**	**0.47**	**3.04**	**1.38**
		***	0.57	3.67	1.52	0.03	2.79	1.01

Notes: Subscript letter *m* and *v* represent the results of modeling and validation. The bold line is the optimal model for estimating SSC and SWC. R, G, B and Gr mean red, green, blue and gray. SSC and SWC represent soil salt content and soil water content. * means $P < 0.05$, ** means $P < 0.01$, *** means $P < 0.001$

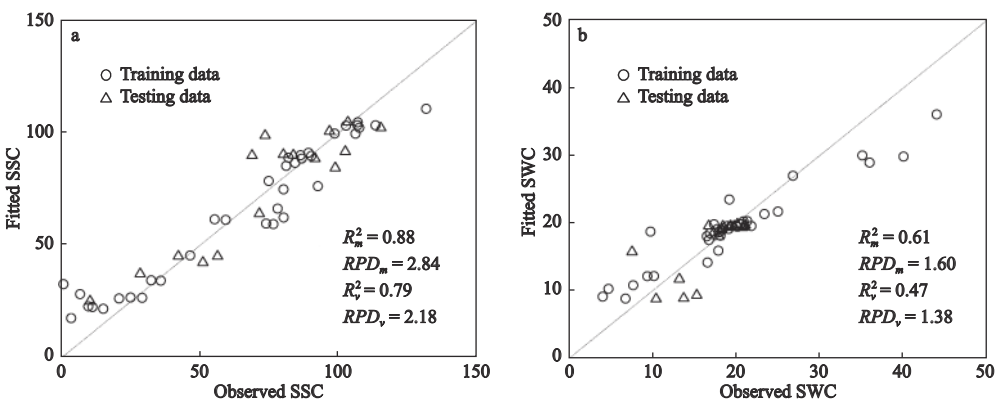

Fig. 5 Scatter diagram of observed and predicted (a) soil salt content and (b) soil water content in the coast area of Yancheng City of Jiangsu Province, China

further, seals the soil surface and prevents soil water evaporation (Xu et al., 2021b). Therefore, soil salt and soil water coexist in coastal area, which is different from other inland salt types (Ren et al., 2016; Xu et al., 2019). Increasing soil salt content brightens the soil surface, and increasing soil water content darkens the soil surface.

Though soil salt content has significantly positive correlation with the average brightness value, there are also many brightness levels negatively related with soil salt content (Xu et al., 2020). To explain this, we plotted the proportion of each brightness level for each color component in total digital images and showed in Fig. 6. It indicated that most pixels had comparatively high brightness values, and only a few pixels had small brightness values. Hence, the correlation coefficients at the high brightness range possess the large weight. Back to look at the Fig. 4, the positive relationship between soil salt content and brightness levels is mainly distributed at the high-brightness range (about 180–255). This brightness range happens to be the brightness region with the largest pixel proportions. Consequently, the high positive correlation coefficients with the most image pixels make the soil salt content be significantly positive with average brightness value. As to soil water content, there are three brightness ranges having the positive correlation and one brightness range having the negative correlation. In terms of pixel proportion, only one positive correlation at the high-brightness range (about 200–255) and one negative correlation at the middle-brightness range (about 130–200) matter. The positive correlation coefficients are smaller than the negative correlation coefficients, but the positive ones have more pixels than the negative ones. The comprehensive result makes soil water content appear to positively weak correlation with average brightness value. Soil salt content relates significantly to many more brightness levels than soil water content does, especially at the high-brightness range where the most pixels concentrated. These phenomena imply that soil salt content can be estimated more accurately than soil water content.

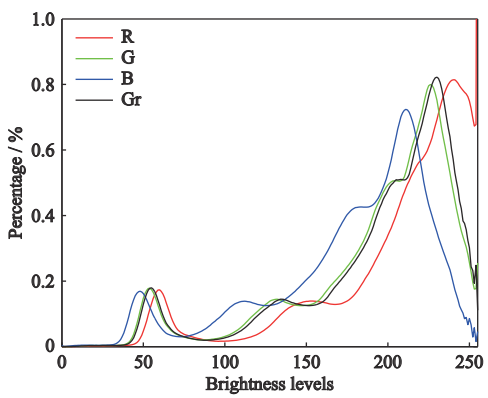

Fig. 6 The proportion of each brightness level for each color component in total digital images in the coast area of Yancheng City of Jiangsu Province, China. R, G, B and Gr mean red, green, blue and gray

4.2 Effects of variable selection on models

Variable selection is commonly used for building models with a great many of variables, especially for spectral models (Rossel and Behrens, 2010; Shi et al., 2014; Vohland et al., 2014; Xu et al., 2016; Xu et al., 2020). We dissect every pixel in the image, and consider that the brightness value of each pixel in an image can reflect the soil properties. Hence all the brightness levels should be the potential variables for modeling soil properties. However, not all of them are very relevant with soil properties, so variable selection is necessary to screen out the useful variables for developing accurate models. P value, an important index for significance, is able to mark the correlative brightness levels and therefore can be an efficient path to select useful brightness levels. Setting different P values will identify the different brightness levels chosen as the input variables of models. The number of variables at $P < 0.05$ significance level is surely more than the variable number at $P < 0.01$ and $P < 0.001$ levels, but the variables with the best correlation concentrated at $P < 0.001$ level. From the Table 2, we can see that many brightness levels are involved even at $P < 0.001$ level, so it is difficult to say which one works best. Through the modeling and testing of random forest models, we determine that soil salt content can be well estimated with blue color component and the brightness levels identified at $P < 0.05$ level, and soil water content can be estimated barely satisfactory with gray color component and the brightness levels selected at $P < 0.01$ level.

4.3 Potential applications

Digital camera as a scientific tool had received much attention in soil prediction for a long time (Adamsen et al., 1999; Persson, 2005; d'Oleire-Oltmanns et al., 2012; Moonrungsee et al., 2015; Xu et al., 2021a). However, most of them conducted in the laboratory, and few had practical application. Our study is completely carried on in the field, the data and image process are conducive to build soil properties inversion models for in-situ conditions. This study focused on the sample points, and had certain meanings for precise field management. With

the rapid development of unmanned aerial vehicles (UAV), unmanned aerial systems (UAS) for monitoring soil conditions is easy to build, and has great practical value and bright prospects on large scales. Ongoing work will focus on the practical application with the combination of digital camera and UAV. Additionally, the three color components (RGB) extracted from digital images are commonly consistent with the channels of many satellite sensors (Cantrell et al., 2010). This indicates that digital images may have some relation with remote sensing data and further have great potential for large-scale application.

5 Conclusions

Digital image is a comprehensive reflection of soil surface condition. Soil salt content and soil water content influence comprehensively the surface soil brightness, which will reflect on the digital images. In light of this phenomenon, we believe that soil salt content and soil water content can be modeled with image brightness. We dissected each brightness levels and discovered the relationship between soil properties and soil brightness, and develop the inversion models with random forest algorithm. Our findings indicated that soil salt content was better estimated by digital images (R_v^2 = 0.79, $RMSE_v$ = 12 g/kg, and RPD_v = 2.18), and soil water content inversion model was barely satisfied (R_v^2 = 0.47, $RMSE_v$ = 3.04 %, and RPD_v = 1.38). This work provides an effective approach to assess soil properties using digital camera images, and we can further explore the relationship between soil properties and digital images, which helps to promote the development precision agriculture and land management in coastal area.

References

Adamchuk V I, Rossel R A V, 2011. Precision agriculture: proximal soil sensing. In: Gliński J et al. (eds.) *Encyclopedia of Agrophysics. Encyclopedia of Earth Sciences Series*. Dordrecht: Springer, 650–656. doi: 10.1007/978-90-481-3585-1_126

Adamchuk V, Allred B, DoolittleJ et al., 2015. Tools for proximal soil sensing. Soil Survey Staff, C. Ditzler, and L. West, eds. Soil survey manual. United States Department of Agriculture Handbook (18).

Adamsen F J, Pinter P J, Barnes E M et al., 1999. Measuring wheat senescence with a digital camera. *Crop Science*, 39(3): 719–724. doi: 10.2135/cropsci1999.0011183X003900030019x

Aitkenhead M, Donnelly D, Coull M et al., 2016. Estimating soil properties with a mobile phone. In: Hartemink A E, Minasny B (eds). *Digital Soil Morphometrics*, Switzerland: Springer, 89–110. doi: 10.1007/978-3-319-28295-4_7

Barrett B W, Dwyer E, Whelan P, 2009. Soil moisture retrieval from active spaceborne microwave observations: an evaluation of current techniques. *Remote Sensing*, 1(3): 210–242. doi: 10.3390/rs1030210

Breiman L,, 2001. Random forests. *Machine Learning*, 45(1): 5–32. doi: 10.1023/A:1010933404324

Cantrell K, Erenas M M, De Orbe-Payá I et al., 2010. Use of the hue parameter of the hue, saturation, value color space as a quantitative analytical parameter for bitonal optical sensors. *Analytical Chemistry*, 82(2): 531–542. doi: 10.1021/ac901753c

Chang C W, Laird D A, Mausbach M J et al., 2001. Near-infrared reflectance spectroscopy-principal components regression analyses of soil properties. *Soil Science Society of America Journal*, 65(2): 480–490. doi: 10.2136/sssaj2001.652480x

D'Oleire-Oltmanns S, Marzolff I, Peter K D et al., 2012. Unmanned Aerial Vehicle (UAV) for monitoring soil erosion in Morocco. *Remote Sensing*, 4(11): 3390–3416. doi: 10.3390/rs4113390

Fang Renjian, Shen Yongming, Shi Haidong, 2015. The changes of coastal wetland landscape pattern based on the characteristics of reclamation: a case study in coastal wetland of Yancheng, Jiangsu province, China. *Acta Ecologica Sinica*, 35(3): 641–651. (in Chinese)

Farifteh J, 2011. Interference of salt and moisture on soil reflectance spectra. *International Journal of Remote Sensing*, 32(23): 8711–8724. doi: 10.1080/01431161.2010.549522

Fu Y Y, Taneja P, Lin S M et al., 2020. Predicting soil organic matter from cellular phone images under varying soil moisture. *Geoderma*, 361: 114020. doi: 10.1016/j.geoderma.2019.114020

Islam K, McBratney A, Singh B, 2004. Estimation of soil colour from visible reflectance spectra. Proceedings of Supersoil.

Ivushkin K, Bartholomeus H, Bregt A K et al., 2019. Global mapping of soil salinity change. *Remote Sensing of Environment*, 231: 111260. doi: 10.1016/j.rse.2019.111260

Jackson M L, 2005. Soil chemical analysis: Advanced course. UW-Madison Libraries parallel press.

Metternicht G, Zinck J A, 2008. *Remote Sensing of Soil Salinization: Impact on Land Management*. Boca Raton: CRC Press.

Metternicht G I, Zinck J A, 2003. Remote sensing of soil salinity: potentials and constraints. *Remote Sensing of Environment*, 85(1): 1–20. doi: 10.1016/S0034-4257(02)00188-8

Moonrungsee N, Pencharee S, Jakmunee J, 2015. Colorimetric analyzer based on mobile phone camera for determination of available phosphorus in soil. *Talanta*, 136: 204–209. doi: 10.1016/j.talanta.2015.01.024

Persson M, 2005. Estimating surface soil moisture from soil color using image analysis. *Vadose Zone Journal*, 4(4): 1119–1122. doi: 10.2136/vzj2005.0023

Puzachenko Y G, Puzachenko M Y, Kozlov D N et al., 2004. Soil structure analysis with the use of digital color images. *Eurasian Soil Science*, 37(2): 109–121.

Qadir M, Schubert S, Ghafoor A et al., 2001. Amelioration strategies for sodic soils: a review. *Land Degradation & Development*, 12(4): 357–386. doi: 10.1002/ldr.458

Ren J H, Li X J, Zhao K et al., 2016. Study of an on-line measurement method for the salt parameters of soda-saline soils based on the texture features of cracks. *Geoderma*, 263: 60–69. doi: 10.1016/j.geoderma.2015.08.039

Rhoades J D, Ingvalson R D, 1971. Determining salinity in field soils with soil resistance measurements. *Soil Science Society of America Journal*, 35(1): 54–60. doi: 10.2136/sssaj1971.03615995003500010020x

Rossel R A V, Behrens T, 2010. Using data mining to model and interpret soil diffuse reflectance spectra. *Geoderma*, 158(1-2): 46–54. doi: 10.1016/j.geoderma.2009.12.025

Shi T Z, Chen Y Y, Liu H Z et al., 2014. Soil organic carbon content estimation with laboratory-based visible-near-infrared reflectance spectroscopy: feature selection. *Applied Spectroscopy*, 68(8): 831–837. doi: 10.1366/13-07294

Su C H, Zhang J, Gruber A et al., 2016. Error decomposition of nine passive and active microwave satellite soil moisture data sets over Australia. *Remote Sensing of Environment*, 182: 128–140. doi: 10.1016/j.rse.2016.05.008

Viscarra Rossel R A, Fouad Y, Walter C, 2008. Using a digital camera to measure soil organic carbon and iron contents. *Biosystems Engineering*, 100(2): 149–159. doi: 10.1016/j.biosystemseng.2008.02.007

Viscarra Rossel R A, McBratney A B, Minasny B, 2010. *Proximal Soil Sensing*. Dordrecht: Springer. doi: 10.1007/978-90-481-8859-8

Viscarra Rossel R A, Bouma J, 2016. Soil sensing: a new paradigm for agriculture. *Agricultural Systems*, 148: 71–74. doi: 10.1016/j.agsy.2016.07.001

Vohland M, Ludwig M, Thiele-Bruhn S et al. , 2014. Determination of soil properties with visible to near- and mid-infrared spectroscopy: effects of spectral variable selection. *Geoderma*, 223–225: 88–96. doi: 10.1016/j.geoderma.2014.01.013

Wang J Z, Ding J L, Yu D L et al., 2019. Capability of Sentinel-2 MSI data for monitoring and mapping of soil salinity in dry and wet seasons in the Ebinur Lake region, Xinjiang, China. *Geoderma*, 353: 172–187. doi: 10.1016/j.geoderma.2019.06.040

Wang J Z, Ding J L, Yu D L et al., 2020. Machine learning-based detection of soil salinity in an arid desert region, Northwest China: a comparison between Landsat-8 OLI and Sentinel-2 MSI. *Science of the Total Environment*, 707: 136092. doi: 10.1016/j.scitotenv.2019.136092

Wang L L, Qu J J, 2009. Satellite remote sensing applications for surface soil moisture monitoring: a review. *Frontiers of Earth Science in China*, 3(2): 237–247. doi: 10.1007/s11707-009-0023-7

Werner A D, Bakker M, Post V E A et al., 2013. Seawater intrusion processes, investigation and management: Recent advances and future challenges. *Advances in Water Resources*, 51: 3–26. doi: 10.1016/j.advwatres.2012.03.004

Wu C W, Xia J X, Yang H et al., 2018. Rapid determination of soil organic matter content based on soil colour obtained by a digital camera. *International Journal of Remote Sensing*, 39(20): 6557–6571. doi: 10.1080/01431161.2018.1460511

Wulf H, Mulder T, Schaepman M E et al. , 2014. *Remote Sensing of Soils*. Switzerland: University of Zurich.

Xu C, Zeng W Z, Huang J S et al., 2016. Prediction of soil moisture content and soil salt concentration from hyperspectral laboratory and field data. *Remote Sensing*, 8(1): 42. doi: 10.3390/rs8010042

Xu L, Zheng C L, Wang Z C et al., 2019. A digital camera as an alternative tool for estimating soil salinity and soil surface roughness. *Geoderma*, 341: 68–75. doi: 10.1016/j.geoderma.2019.01.028

Xu L, Viscarra Rossel R A, Lee J et al., 2020. A simple approach to estimate coastal soil salinity using digital camera images. *Soil Research*, 58(8): 737–747. doi: 10.1071/SR20009

Xu L, Wang H, Qiu S Y et al., 2021a. Coastal soil salinity estimation based digital images and color space conversion. *Spectroscopy and Spectral Analysis*, 41(8): 2409–2414. (in Chinese)

Xu L, Wang Z C, Hu J S et al., 2021b. Estimation of soil salinity under various soil moisture conditions using laboratory based thermal infrared spectra. *Journal of the Indian Society of Remote Sensing*, 49(4): 959–969. doi: 10.1007/s12524-020-01271-9

Yang R M, Guo W W, 2019. Using Sentinel-1 imagery for soil salinity prediction under the condition of coastal restoration. *IEEE Journal of Selected Topics in Applied Earth Observations and Remote Sensing*, 12(5): 1482–1488. doi: 10.1109/JSTARS.2019.2906064

Yashchenko A S, Bobrov P P, 2016. Impact of the soil moisture distribution in the top layer on the accuracy moisture retrieval by microwave radiometer data. *IEEE Transactions on Geoscience and Remote Sensing*, 54(9): 5239–5246. doi: 10.1109/TGRS.2016.2559162

Yue J B, Tian J, Tian Q J et al., 2019. Development of soil moisture indices from differences in water absorption between shortwave-infrared bands. *ISPRS Journal of Photogrammetry and Remote Sensing*, 154: 216–230. doi: 10.1016/j.isprsjprs.2019.06.012

Zanetti S S, Cecílio R A, Alves E G et al., 2015. Estimation of the moisture content of tropical soils using colour images and artificial neural networks. *Catena*, 135: 100–106. doi: 10.1016/j.catena.2015.07.015

Zhu Y J, Wang Y Q, Shao M A et al., 2011. Estimating soil water content from surface digital image gray level measurements under visible spectrum. *Canadian Journal of Soil Science*, 91(1): 69–76. doi: 10.4141/cjss10054